ELSEVIER

Journal of Materials Processing Technology 117 (2001) 409–417

Journal of Materials Processing Technology

www.elsevier.com/locate/jmatprotec

# Internal-stress plasticity in titanium by cyclic alloying/dealloying with hydrogen

Peter Zwigl*, David C. Dunand

*Department of Materials Science and Engineering, Northwestern University, Evanston, IL 60208, USA*

**Abstract**

Internal-stress plasticity is a deformation mechanism where an externally applied stress biases internal mismatch stresses. We report here a novel method to induce internal-stress plasticity in titanium: a reversible change of chemical composition (at constant temperature) is produced by cyclic alloying/dealloying with hydrogen, rather than by thermal cycling (at constant composition) which induces the well-known phenomenon of transformation-mismatch plasticity in titanium. We demonstrate that chemical cycling with hydrogen, which induces internal stresses by both swelling mismatch and transformation mismatch, results in large, reproducible strain increments in the direction of the applied stress. We systematically explore different processing variables (applied stress, temperature, as well as hydrogen concentration, cycling rate and flow rate) and discuss our results in the light of previous studies on internal-stress plasticity induced by thermal cycling. © 2001 Published by Elsevier Science B.V.

*Keywords:* Titanium; Hydrogen; Superplasticity; Plasticity; Creep; Phase transformations

## 1. Introduction

Thermochemical processing (TCP) is a technique using hydrogen as a temporary alloying element in, e.g., titanium and its alloys to improve hot-working and to produce novel microstructures with unique properties, as reviewed in [1,2]. Because of the very high diffusivity of hydrogen, α-Ti can be rapidly alloyed with hydrogen by exposure to a hydrogen-bearing atmosphere, leading to the formation of the mechanically weak β-Ti phase (Fig. 1). After hot-working in the β-Ti phase, often under superplastic conditions, hydrogen is removed by annealing in vacuum or inert gas and the α-Ti original microstructure is recovered.

Internal-stress plasticity (ISP) is another mechanism used to increase the deformation rate of metals and alloys, which also can lead to superplastic elongations, as reviewed in [3,4]. It relies on the creation of internal stresses produced during thermal cycling by the mismatch in thermal expansion between grains (e.g., in polycrystalline Zn) or between phases (e.g., in Al–SiC composites). Alternatively, internal stresses can be produced during a phase transformation when the two coexisting allotropes have different densities. Transformation plasticity and transformation superplasticity by thermal cycling has been observed in many allotropic metals and alloys [5] and is particularly well-studied in Ti subjected to thermal α–β cycling [5–7].

We describe in the present paper a third approach, which consists in deforming a titanium specimen while simultaneously subjecting it to multiple alloying/dealloying cycles with hydrogen. Like TCP, this process uses temporary alloying with hydrogen, and like ISP, the underlying deformation mechanism is based on the superposition of external and internal stresses. The new method uses internal stresses occurring during the alloying/dealloying process to accelerate deformation of titanium (as in ISP), rather than relying on the hydrogen-induced transformation to produce a weaker, easily deformed phase after full alloying with hydrogen (as in TCP). Because the new method uses hydrogen to induce internal stresses, it can be coined ''chemically induced internal-stress plasticity'', in analogy to the well-known thermally induced ISP. The present paper systematically experimentally investigates chemically induced ISP in titanium occurring isothermally by cyclic alloying–dealloying with hydrogen, and compares results to thermally induced ISP produced by cyclic heating–cooling.

## 2. Experimental procedures

Tensile specimens of unalloyed titanium (99.7% pure, from Alpha Aesar, MA) were machined with a gauge length of 28–52 mm and a rectangular cross-section of 5.4–6.0 mm

* Corresponding author. Present address: Intel Corporation, 1900 Prairie City Rd., Folson, CA 95630, USA.

0924-0136/01/$ – see front matter © 2001 Published by Elsevier Science B.V.
PII: S0924-0136(01)00801-9

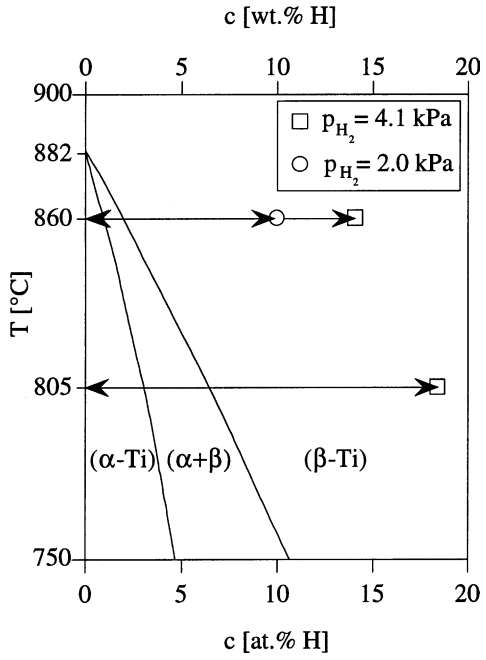


Fig. 1. Ti–H phase diagram [9] illustrating chemical cycles used in the present study of chemically induced ISP ($p_{H_2} = 0 \leftrightarrow 2.0$ kPa or $0 \leftrightarrow 4.1$ kPa) as well a typical thermal cycles used in the literature for thermally induced ISP.

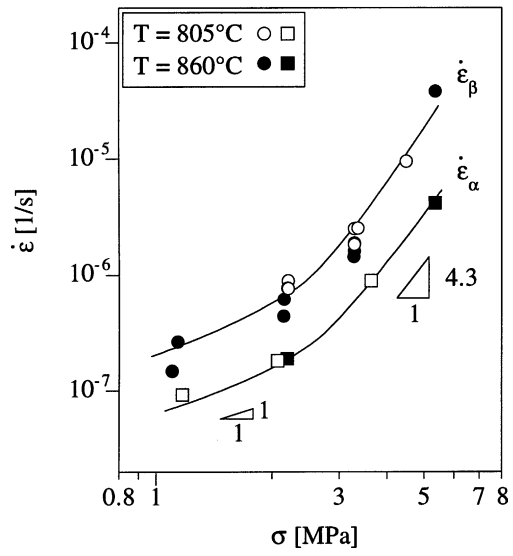


Fig. 2. Stress-dependence of the isothermal steady-state creep rate at 805 and 860°C for α-Ti ($p_{H_2} = 0$ kPa) and β-Ti ($p_{H_2} = 4.1$ kPa).

width and 1.9–2.6 mm thickness. Testing was performed at 805 and 860°C (well below the transus at 882°C) in a custom-designed creep apparatus [8] allowing the application of small tensile stresses under a flowing atmosphere. The gas entering the apparatus could be changed from high-purity 99.999% Ar to a gas mixture Ar–4 vol.% $H_2$. A hydrogen cycle thus consisted of two segments of equal duration under an Ar atmosphere with $H_2$ partial pressures of 0 and 4.1 kPa, respectively. Hydrogen charging (alloying) and discharging (dealloying) occurred during each segment, with a maximum possible hydrogen concentration in titanium of 18.3 at.% at 805°C and 14.3 at.% at 860°C [9], well within the β-Ti field (Fig. 1). The gas flow-rate was constant at 1.22 l/min (standard volume), corresponding to a replacement of apparatus gas volume every 30 s. The temperature of the specimen was controlled within ±2°C by a thermocouple (K- or R-type) positioned at the surface of the gauge section or the pull-head and independently measured by a second thermocouple located at the specimen gage surface. Specimen deformation was recorded continuously at the cold end of the lower pullrod, where a load cell also measured the force applied on the specimen with a stress accuracy of ±0.05 MPa.

## 3. Results and discussion

### 3.1. Isothermal creep at constant composition

Fig. 2 shows the stress dependence of the steady-state creep rate at 805 and 860°C for H-free α-Ti and fully hydrogenated β-Ti, the latter creeping three to five times faster than the former, as qualitatively expected from the higher diffusion constant of the BCC lattice of β-Ti [10]. Stress exponents tend towards values of $n \approx 1$ at low stresses and $n \approx 4.3$ at high stresses, with a transition in the range $\sigma = 1.5-3.5$ MPa, in general agreement with the calculated transition between diffusional and dislocation creep (near 1 MPa for a 20 μm grain size [10]). Fig. 2 does not, however, shows the doubling in creep rate from 805 to 860°C which would be expected from the value of the bulk diffusion activation energy of Ti [10]. This may be due to minor differences in microstructure between specimens and/or measurement errors at these relatively low creep rates.

### 3.2. Deformation mechanisms active upon chemical cycling

Over a full H-cycle, four types of strains are developed:

1. Lattice swelling strain $|\varepsilon_S|$ due to swelling upon H-charging (respectively, deswelling upon H-discharging) with volume mismatch $(\Delta V/V)_S$.
2. Lattice transformation strain $|\varepsilon_T|$ from the volume mismatch $(\Delta V/V)_T$ between α- and β-Ti upon transformation.
3. Plastic strain from creep deformation $\Delta\varepsilon_c$ in the absence of internal mismatch (i.e., at constant composition after H-charging or H-discharging are complete for each segment).
4. Plastic strain $\Delta\varepsilon$ caused by internal mismatch accommodation (ISP).

The signs of the reversible lattice strains caused by mechanisms (1) and (2) change for the H-charging and H-discharging segments, so that no permanent deformation is accumulated after a full H-cycle (or only very small strains

in the presence of ratchetting [11]). On the other hand, plastic strains due to mechanisms (3) and (4) always act in the direction of the applied stress, and are thus cumulative. We note that while ISP (mechanism (4)) is an independent contribution to strain, it relies on mechanisms (1) and (2) to produce internal mismatch stresses and on mechanism (3) to relax them.

The magnitude of the internal volume mismatch produced by the two independent mechanisms (2) and (1) are respectively $(\Delta V/V)_T = 0.48\%$ [12] for the allotropic mismatch and $(\Delta V/V)_S = 1.95\%$ for the swelling mismatch at 860°C (with contribution of 0.16 and 1.79% in the α- and β-phases, respectively [11]). Thus, for the present conditions of temperature and $H_2$ partial pressures, the majority of the mismatch is produced by β-Ti lattice swelling, while mismatch from the phase transformation is smaller (but non-negligible). The signs of these mismatches are however opposite, so uptake of hydrogen leads to the following sequential volume changes at 860°C: (i) a modest 0.16% swelling of α-Ti, (ii) a 0.48% allotropic contraction and (iii) a large 1.79% swelling of β-Ti. This chain of events and the signs of the strains are reversed upon H-discharging. The state of internal stress is thus complex, as the allotropic mismatch partially cancels the alloying mismatch, and as the concentration profile is time-dependent. It is beyond the scope of the present paper to model this complicated coupled diffusion-mechanics problem, which will be treated in future publications and which was also addressed in [11] for the simpler case where no external stress is applied (i.e., ratchetting induced by chemical cycling). In the following, we probe experimentally the effect of stress, temperature, cycling frequency, hydrogen concentration and hydrogen flow rate, which all affect the diffusion profile in titanium and thus the distribution of internal stresses and eventual specimen macroscopic strain.

### 3.3. Stress dependence of ISP induced by chemical cycling

The strain history of a specimen cycled four times at 805°C under different stresses ranging from 0.4 to 3.3 MPa is shown in Fig. 3(a) and (b) for H-charging and H-discharging segments, respectively. Fig. 3(c) and (d) shows the strain history for three cycles at 860°C for stresses from 1.1 to 5.4 MPa. Prior to cycling, the H-free specimens were subjected to creep at $\sigma = 1.2$ MPa and $T = 805$°C and at $\sigma = 2.2$ MPa and $T = 860$°C (data given in Fig. 2). The strain curves in Fig. 3(a)–(d) is dominated by swelling and deswelling at short times when the H-concentration changes rapidly, and by creep at long times when the H-concentration is constant. The total strain increment $\Delta\varepsilon_{tot}$ accumulated at the end of each cycle (consisting of consecutive H-charging and H-discharging segments) consists of plastic strain due to creep $\Delta\varepsilon_c$ and to ISP $\Delta\varepsilon$, since the strain contributions from hydrogen swelling $|\varepsilon_S|$ and transformation strain $|\varepsilon_T|$ are reversible and cancel at the end of the cycle. The strain increment $\Delta\varepsilon$ due to ISP can then be found by subtracting the creep contribution $\Delta\varepsilon_c$ accumulated during the cycle time from the measured total strain increment $\Delta\varepsilon_{tot}$. Multiplying the steady-state creep rate measured at the end of the time interval (H-charging or H-discharging, respectively) by the half-cycle time gives the value of $\Delta\varepsilon_c$. This so-called creep correction overestimates creep during H-charging segments, as the material is first in the α-phase where creep rates are three to five times smaller than for β-Ti (Fig. 2). However, on H-discharging the creep strains are underestimated because the material deforms in the β-state prior to the phase transformation. For stresses below 4 MPa, $\Delta\varepsilon_c$ is small relative to $\Delta\varepsilon$, so such errors are unimportant.

Fig. 4 shows the creep-corrected strain increment $\Delta\varepsilon$ for a complete H-cycle at each temperature as a function of the applied stress. The data can be fitted by a straight line with a slope of $d(\Delta\varepsilon)/d\sigma = 7.0\,GPa^{-1}$ and an intercept of $-0.05\%$, indicative that a small ratchetting strain would accrue after each cycle for specimens with no externally applied stress. Fig. 4 contains all data given in Fig. 3(a)–(d), except for $\sigma = 5.4$ MPa, because this cycle involved a large amount of creep, whose correction is too imprecise. In Fig. 5, the strain increment accumulated at the end of H-charging segments, $\Delta\varepsilon_{tot,c}$, and H-discharging segments, $\Delta\varepsilon_{tot,d}$, are plotted against the applied stress. At the stress levels shown in Fig. 5, isothermal creep can be neglected so that the strain increments are $\Delta\varepsilon_{tot,c} = |\varepsilon_S| - |\varepsilon_T| + \Delta\varepsilon_1$ for H-charging and $\Delta\varepsilon_{tot,d} = |\varepsilon_S| - |\varepsilon_T| + \Delta\varepsilon_1$ for H-discharging. The slopes of the curves for H-charging and H-discharging are respectively $d(\Delta\varepsilon_{tot,c})/d\sigma = 3.7$ and $d(\Delta\varepsilon_{tot,d})/d\sigma = 3.8\,GPa^{-1}$. Within experimental error, the sum of these slope is equal to the value $d(\Delta\varepsilon)/d\sigma = 7.0\,GPa^{-1}$ for complete cycles (Fig. 4), as expected. Also, the individual slopes are about equal to each other, indicating that each H-charging and H-discharging segment contributes the same ISP strain increment, as reported in other studies (e.g., [8]) of thermally induced ISP where equal strain increments are observed upon heating and cooling segments of thermal cycles. Finally, extrapolating the best-fit lines in Fig. 5 to $\sigma = 0$ gives intercepts whose magnitude represents $|\varepsilon_S| - |\varepsilon_T|$ and decreases with increasing temperature, as expected from the lower H-solubility and associated lower swelling at higher temperature. The sum of the intercepts for two charging/discharging segments takes non-zero values ($-0.11\%$ at 805°C and $-0.13\%$ at 860°C), in rough agreement with the value $-0.05\%$ extrapolated from Fig. 4. However, the value at 860°C agrees well with a recent ratchetting study [11] performed on Ti subjected to similar H-cycling at 860°C, where ratchetting strains of $-0.14\%$ were found after a full H-cycle.

Finally, sharp, reproducible temperature changes were observed at the specimen heads upon H-charging (ca. −3°C) and H-discharging (ca. +3°C), followed by a gradual return in about 15 min to the nominal temperature. Possible causes for these thermal excursions include the enthalpy of H-dissolution and α–β transformation, as well as the change in gas conduction and convection upon addition of hydrogen.

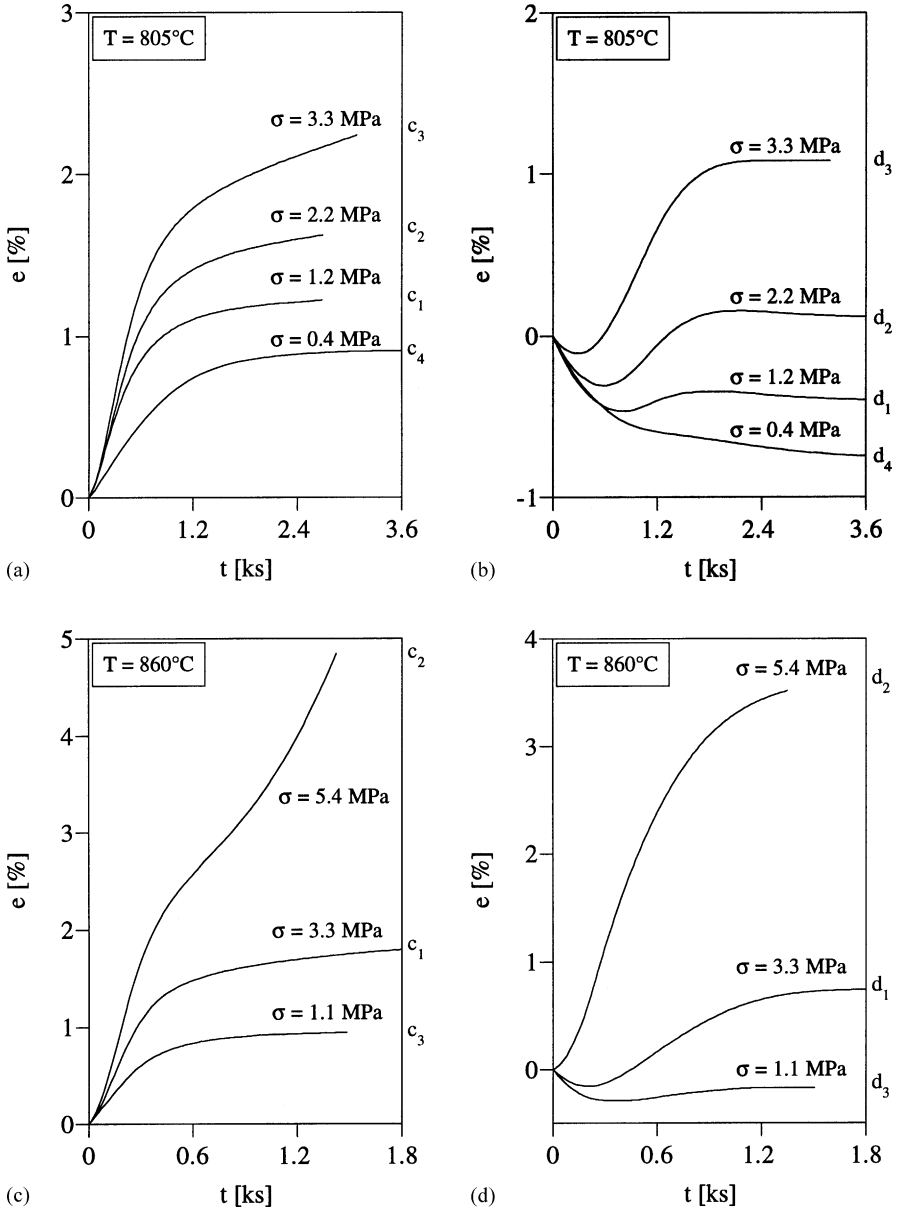


Fig. 3. Strain history at different stresses for segments of H-charging ($p_{H_2} = 4.1\,\text{kPa}$) and H-discharging ($p_{H_2} = 0\,\text{kPa}$) at (a,b) $T = 805°\text{C}$ and (c,d) $T = 860°\text{C}$. Segments are marked with c and d, respectively, with the cycle number as subscript.

### 3.4. Strain history for multiple chemical cycles

Fig. 6 shows the strain history of nine consecutive H-cycles for a constant stress of 2.25 MPa at 805°C. H-cycling was done at a frequency of $3\,\text{h}^{-1}$ giving an average total strain increment per cycle $\Delta\varepsilon_{\text{tot}} = 1.04 \pm 0.08\%$ and a stress-normalized total strain increment $\Delta\varepsilon_{\text{tot}}/\sigma = 4.6 \pm 0.3\,\text{GPa}^{-1}$. After creep-correction, an ISP strain increment $\Delta\varepsilon = 0.94 \pm 0.08\%$ is found, somewhat lower than the values $\Delta\varepsilon = 1.45\%$ shown in Fig. 4 for much slower cycles. During the relatively rapid cycling shown in Fig. 6, the total strain increments decreased with the number of cycles, giving for example $\Delta\varepsilon_{\text{tot}} = 1.15\%$ for the first cycle and $\Delta\varepsilon_{\text{tot}} = 0.84\%$ for the last cycle. This is because the cycling frequency was too high to completely eliminate all hydrogen at the end of the discharging segments, leading to a steady increase in hydrogen after each cycle and thus a steady decrease in internal mismatch. Indeed, according to Fig. 3(b), the time for complete H-discharging at 805°C is approximately 30 min, much longer than the segment duration of 10 min for the cycles shown in Fig. 6.

Fig. 7 depicts the strain history of the same specimen subjected to three low-frequency segments ($c_{24}$ in 30 min, $d_{24}$ in 50 min, $c_{25}$ in 23 min), which followed the nine high-frequency cycles shown in Fig. 6 (with 10 min segments, the last four of which are also shown in Fig. 7). Also, Fig. 7 illustrates that creep of α-Ti is insignificant after multiple cycling ($u_{24}$), from which it can be concluded that the α-Ti

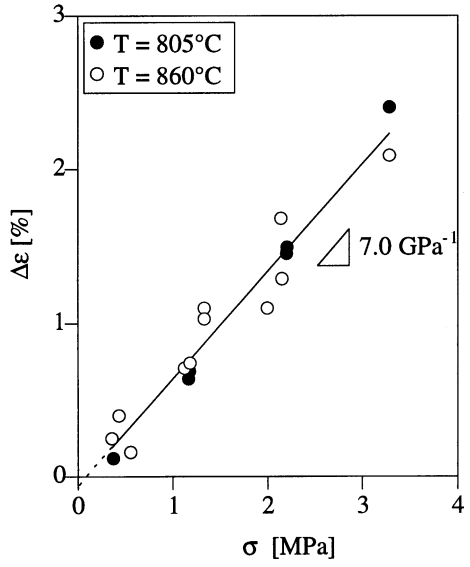


Fig. 4. Creep-corrected ISP strain increment as a function of applied stress for H-cycles with $p_{H_2} = 0 \leftrightarrow 4.1$ kPa, $v \leq 1.35\,h^{-1}$ at $T = 805$ and 860°C.

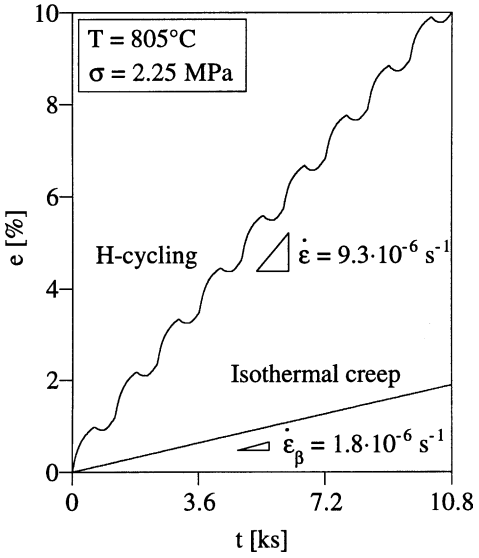


Fig. 6. Strain history upon H-cycling at constant stress $\sigma = 2.25$ MPa and temperature $T = 805$°C for nine H-cycles with $p_{H_2} = 0 \leftrightarrow 4.1$ kPa and $v = 3\,h^{-1}$, as compared to isothermal creep strain of β-Ti at $T = 805$°C, $p_{H_2} = 4.1$ kPa.

grain size is not significantly refined by H-cycling. Finally, Fig. 7 shows a β-Ti creep rate of $\dot{\varepsilon}_\beta = 1.7{-}1.8 \times 10^{-6}\,s^{-1}$ (segments $c_{24}$ and $c_{25}$) which is somewhat higher than that shown in Fig. 2, probably because steady-state concentration and/or steady-state creep had not been fully attained. This upper-bound value for the β-Ti creep rate is used in Fig. 6 to draw a creep curve for uncycled β-Ti, illustrating the very significant enhancement of creep rate induced by H-cycling, despite the fact that the cycled specimen was in the strong α-Ti phase during part of the cycles.

Fig. 8 illustrates H-cycling at the higher temperature ($T = 860$°C), for a stress of 1.36 MPa, and a high cycling rate of $6\,h^{-1}$. Because of the high cycling frequency (5 min segments) only partial transformation occurred (Fig. 3(d) suggests a discharging time of about 20 min). The total strain increment per cycle is $\Delta\varepsilon_{tot} = 0.28 \pm 0.01\%$ (corresponding to $\Delta\varepsilon_{tot}/\sigma = 2.1\,GPa^{-1}$) or, upon creep correction, $\Delta\varepsilon = 0.20 \pm 0.01\%$ (i.e., $\Delta\varepsilon/\sigma = 1.5\,GPa^{-1}$). The average strain rate is $4.7 \pm 10^{-5}\,s^{-1}$, faster than the isothermal value measured just before cycling (shown in Fig. 8 as a dotted line with $\dot{\varepsilon}_\beta = 2.6 \times 10^{-6}\,s^{-1}$) or the steady-state value ($\dot{\varepsilon}_\beta = 3 \times 10^{-7}\,s^{-1}$, Fig. 2).

A total strain of 63% was reached on one of the specimens which had been subjected to H-cycling and creep. While too

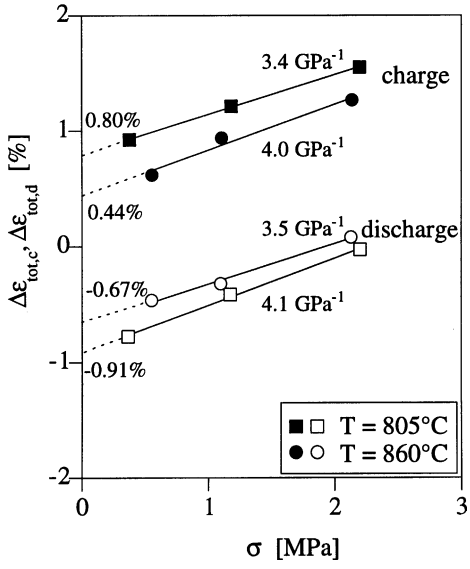


Fig. 5. Total strain increment for H-charging and H-discharging segments as a function of the applied stress at $T = 805$ and 860°C.

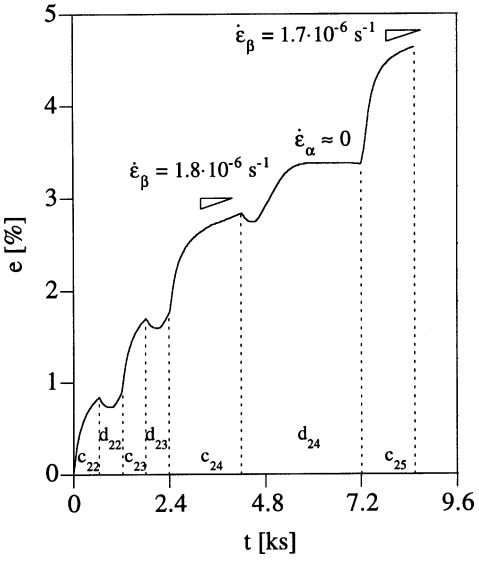


Fig. 7. Strain history and temperature history for high-frequency H-cycles ($c_{22}$–$d_{23}$, given in Fig. 6) followed by three low-frequency cycles ($c_{24}$–$c_{25}$).

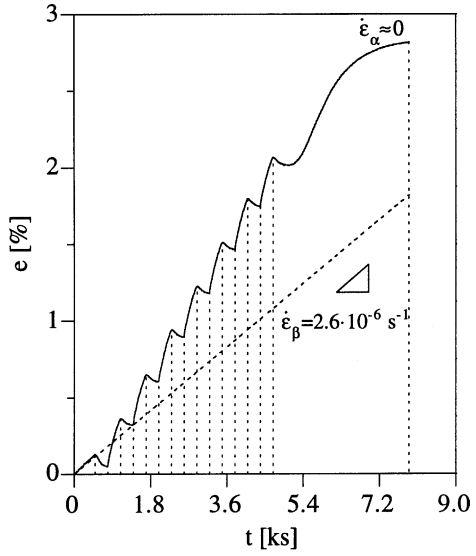


Fig. 8. Strain history and temperature history of H-cycling at constant stress $\sigma = 1.36$ MPa and temperature $T = 860$°C for seven H-cycles with $p_{H_2} = 0 \leftrightarrow 4.1$ kPa and $v = 6\,h^{-1}$, as compared to isothermal creep curve of β-Ti at $T = 860$°C, $p_{H_2} = 4.1$ kPa measured just before cycling.

low to be called superplastic, this strain was achieved with no fracture, indicating that superplastic fracture strains (>100%) are most probably possible by H-cycling.

### 3.5. Effect of temperature, pressure and gas flow rate upon ISP

More detailed information about the underlying mechanisms and their dependencies on processing parameters (temperature, partial pressure and atmosphere flow rate) can be obtained upon superposition of individual H-charging and H-discharging segments, as done in Fig. 3 for different stresses. Fig. 9(a) shows the effect of temperature on the strain history, keeping the other two parameters constant. The higher temperature reduces the magnitude of the strain curves for each segment, because the solubility of hydrogen decreases with temperature. However, the plastic strain accumulated after the whole cycle is nearly identical. Also, as expected from faster diffusion, the higher temperature leads to faster kinetics, as shown by a shorter transient to reach the steady-state creep rate on H-charging and by an earlier onset of plasticity on H-discharging (i.e., the strain minimum occurs earlier).

The dependence of the strain history upon $H_2$ partial pressure at 860°C is shown in Fig. 9(b). The lower partial pressure of 2.0 kPa corresponds to an equilibrium H-concentration of 10.0 at.% [9], sufficient to induce complete transformation to β-Ti (Fig. 1). Fig. 9(b) illustrates that a decrease in $H_2$ partial pressure leads to slower kinetics and lower total cycle plastic strain, as expected from the reduced driving force for diffusion and the lower equilibrium H-concentration.

Finally, Fig. 9(c) displays the strain history for the standard atmosphere flow rate of 1.22 l/min and a reduced rate of 0.14 l/min, for which markedly slower kinetics and lower strain per cycle are observed. This is expected given the much longer transient until the atmosphere is at equilibrium (the time for a change of apparatus gas volume increases from 30 to 260 s) leading to shallower gradients in H-concentration and mismatch strain within the specimen.

### 3.6. Comparison between chemically and thermally induced ISP

A brief qualitative discussion can be based on the model of Greenwood and Johnson [5] developed for the case of transformation-mismatch plasticity induced by thermal cycling about an allotropic temperature. In this model, which has been validated for many materials including Ti [5,7], the ISP strain increment $\Delta\varepsilon$ after a full α–β temperature cycle is

$$\Delta\varepsilon = \frac{4}{3}\left|\frac{\Delta V}{V}\right| \frac{5n}{4n+1}\sigma\left(\frac{2}{3}\left|\frac{\Delta V}{V}\right|\frac{1}{A\,\Delta t}\right)^{-1/n} \quad (1)$$

where $|\Delta V/V|$ is the volume mismatch between the allotropic phases, $\sigma$ the applied stress, and $n$ the stress exponent of the creep law describing the plastic accommodation of the weaker phase (β-Ti). The last term in the right-hand side of Eq. (1) is the average internal stress in the weaker phase, which is expressed as a function of the power-law constant $A$ and the transformation time $\Delta t$ during which both mismatching phases coexist. It follows from Eq. (1) that the strain per cycle normalized by the applied stress $d(\Delta\varepsilon)/d\sigma$ is proportional to $|\Delta V/V|^{1-1/n}$ and $(A\,\Delta t)^{1/n}$, and thus increases with increasing values of $|\Delta V/V|$ and $\Delta t$, and with decreasing values of $n$. Comparing chemically and thermally induced ISP, the internal mismatch $|\Delta V/V|$ is larger for the former because of the additional swelling mismatch. Second, the lower temperature (860°C for H-cycling and about 900°C on average for thermal cycling) translates in a power-law constant $A$ lower by less than a factor 2, calculated from a creep activation energy from [10]. This drop is more than compensated by the longer effective time $\Delta t$ over which mismatch is developed, because H-cycling is controlled by atomic diffusion which is slower than thermal conductivity controlling thermal cycling. Finally, the stress exponent of hydrogenated β-Ti ($n = 1-2$ between 1 and 3 MPa at 860°C, Fig. 2) is lower than for H-free β-Ti ($n = 4.3$ between 0.5 and 3 MPa at 1000–1030°C [6,7]). This qualitative analysis thus predicts that chemical cycling will produce larger ISP strains than thermal cycling. Indeed, Fig. 4 shows a value $d(\Delta\varepsilon)/d\sigma = 7.0\,GPa^{-1}$ upon H-cycling, significantly higher than $d(\Delta\varepsilon)/d\sigma = 2.3\,GPa^{-1}$ reported in three independent studies summarized in [7], where titanium was thermally cycled about its phase transformation. Finally, we note that the lack of difference in $d(\Delta\varepsilon)/d\sigma$ values for H-cycling at 805 and 860°C (Fig. 4) is probably the result of

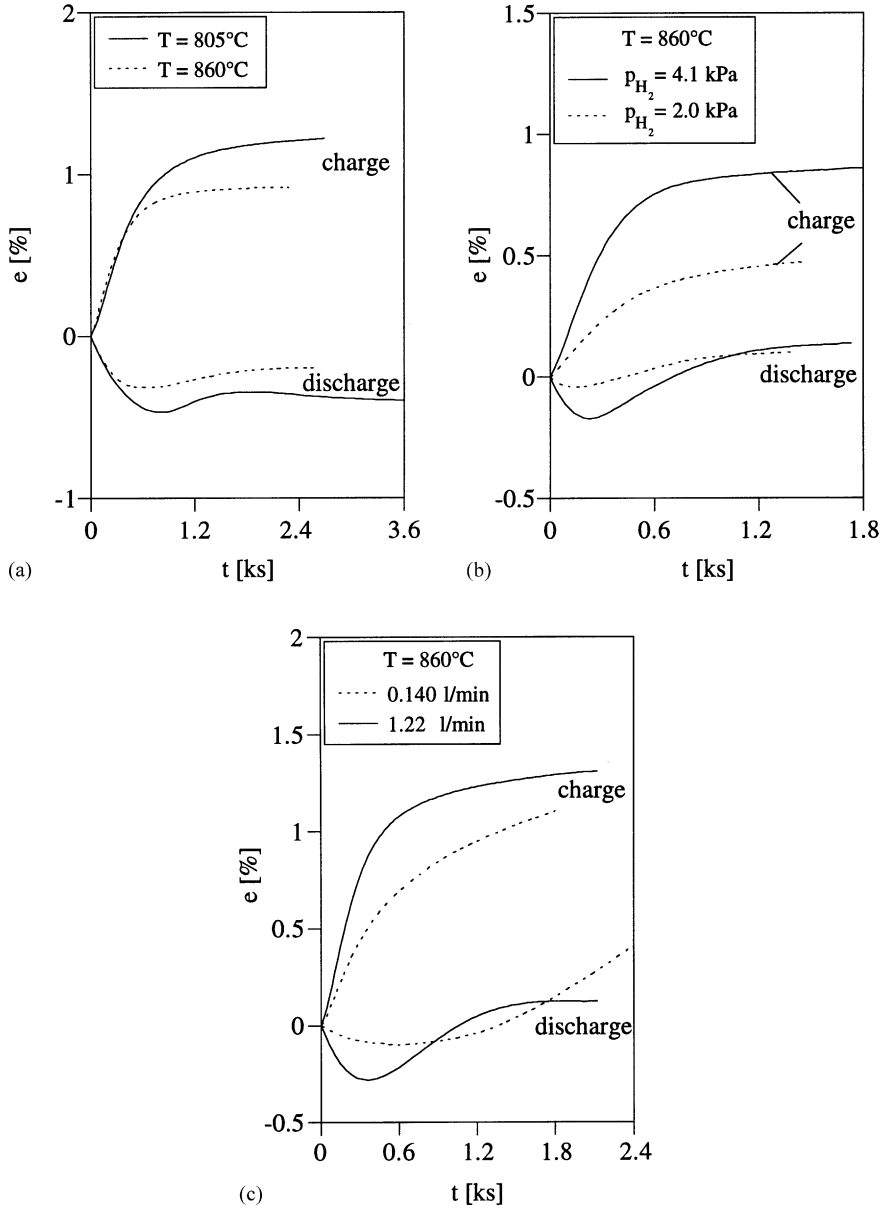


Fig. 9. Strain history upon H-charging and H-discharging for (a) two temperatures ($T = 805$ and 860°C) with constant $\sigma = 1.15$ MPa and $p_{H_2} = 0 \leftrightarrow 4.1$ kPa, (b) for two $H_2$ partial pressures ($p_{H_2} = 0 \leftrightarrow 2.0$ and $0 \leftrightarrow 4.1$ kPa) with constant $T = 860$°C and $\sigma = 2.0$ MPa and (c) for two gas flow rates (0.14 and 1.22 l/min) with constant $T = 860$°C, $\sigma = 2.15$ MPa, $p_{H_2} = 0 \leftrightarrow 4.1$ kPa.

a fortuitous cancellation of effects, since temperature affects the internal mismatch, the creep properties of the accommodating phase and the diffusion kinetics.

Internal-stress superplasticity has good potential to become a technological shape-forming process in materials where microstructural superplasticity is impossible for microstructural or technological reasons. Examples include pure metals where grain-growth cannot be prevented (e.g., pure Zr for the chemical industry or pure Ti for biological implants), composites where reinforcement prevents grain-boundary sliding (e.g., in particulate-reinforced Al/SiC and Ti/TiC composites), and materials where the complex thermomechanical treatment needed to achieve a fine-grain structure is too costly or impossible due to brittleness (e.g., in fiber-reinforced Ti/SiC composites) or due to processing constraints (e.g., in near-net-shape objects produced by casting or powder-metallurgy for which superplastic forming is a final processing step). In such cases, internal-stress superplasticity is a viable forming method with multiaxial deformation rates comparable to those achievable by microstructural superplasticity, as demonstrated in dome-forming experiments performed by thermal cycling of Ti–6Al–4V, Ti–6Al–4V/TiC composites [13] and Al/SiC composites [14]. It is thus appropriate to address whether hydrogen-induced superplasticity by repeated chemical cycling has technological potential as well; in the following, we compare this technique with thermally induced internal-stress superplasticity.

- *Process applicability*. Hydrogen-induced ISP is practical only in materials having a large solubility for hydrogen (to induce swelling mismatch) and/or in materials where a polymorphic transformation or hydride formation occurs upon alloying [15]. There are nine technologically relevant metals with large H-solubility: metals from the group IVA (Ti, Zr, Hf) and VA (V, Nb, Ta) as well as Mg, Pd and U. All the above metals also form hydrides at higher H-concentration, often with very large internal mismatch (e.g., the mismatch between β-Ti and δ-$TiH_2$ is 17.2% [16], as compared to only 0.48% between α- and β-Ti [12]), suggesting that very large strains per cycle may be reached upon β–α H-cycling. Of the above list, the group IVA metals and U further exhibit polymorphic α–β transformations at lower H-concentrations. Finally, many alloys and intermetallic compounds based on these metals also exhibit large hydrogen swelling, hydrogen-induced allotropic transformation and/or hydride precipitation [17]. For comparison, thermally induced transformation plasticity has been demonstrated in the following technologically relevant materials: Fe, Co, Ti, Zr and U [5], of which the first two are not amenable to hydrogen-induced transformation (because of very low solubility and diffusivity for Co and very small difference between the allotropic and eutectoid temperatures for Fe). Thermally induced CTE-mismatch plasticity has been reported in U and Zn [18] (the latter metal is not amenable to H-cycling because of its very low H-solubility) as well as in Al-based composites (which have near-zero H-solubility). However, composites based on the above nine metals with high H-solubility should be amenable to superplastic deformation by H-cycling.
- *Process speed*. In principle, thermally induced mismatch is faster than chemically induced mismatch, because, for all metals listed above, heat conductivity is faster than hydrogen diffusivity for realistic processing conditions. For example, very rapid thermal cycling can be attained by direct sample resistance or induction heating and gas quenching leading to average strain-rates as high as $10^{-2}\,s^{-1}$ for transformation-superplasticity of titanium [19]. Conversely, the driving force for H-cycling is practically limited to cycles between 1 atm $H_2$ and vacuum: the maximum average strain rate can be estimated as $10^{-3}\,s^{-1}$, assuming a 6% strain (measured at 5.4 MPa, Fig. 3(c) and (d)) for H-cycles of 60 s (possibly achievable for very thin specimens). In practice, however, the rate of temperature cycling is expected to be limited by the thermal mass of the apparatus holding the part to be formed. Because H-cycling is isothermal and does not suffer from this practical limitation, its theoretical maximum rate of deformation may be reached more easily in an industrial environment. Furthermore, the average temperature upon H-cycling is lower than upon thermal cycling, which is advantageous for an industrial process.
- *Process control*. Process control under cyclic temperature or composition conditions is inherently more complex than under static conditions. The challenges for thermal cycling forming of complex parts include accurate measurement and control of temperature under dynamic conditions, thermal expansion and contraction of the apparatus holding the part to be formed, and thermal fatigue of the heaters and apparatus. Hydrogen cycling has none of these disadvantages because it can be conducted isothermally (but could also be linked with concomitant thermal cycling). However, special precautions may be required if the $H_2$ partial pressure is above the explosive limit, and if materials susceptible to H-embrittlement are used in the forming apparatus.

Finally, we note that the study of hydrogen-induced ISP is also relevant to materials where this deformation mechanism must be prevented. They include, e.g., Pd membranes used for hydrogen purification and intermetallic alloys for hydrogen storage [17] which are subjected to multiple H-charging/discharging cycles under small external stresses from thermal gradients, vibrations and/or gravity.

## 4. Conclusions

1. ISP was achieved in titanium by superimposing an external stress to internal stresses produced by swelling and transformation mismatch during cyclic alloying/dealloying with hydrogen. This novel mechanism, coined ''chemically induced ISP'', occurs at constant temperature, unlike the well-known thermally induced ISP which relies on temperature cycles.
2. Plastic strain increments are accumulated after each H-cycle. An average strain rate of $3 \times 10^{-5}\,s^{-1}$ was reached at high stress, and optimal cycling conditions may lead to strain rates as high as $10^{-3}\,s^{-1}$.
3. Strain increments are proportional to the applied stress, as expected from the general theory of ISP.
4. Temperature, cycling frequency, maximum hydrogen concentration, and hydrogen flow rate were found to alter the strain increments through their effect on hydrogen diffusion kinetics.

## Acknowledgements

Financial support from the US Army Research Office (grant DAAH04-95-1-0629) and the National Science Foundation (grant DMR-9987593) is gratefully acknowledged. The authors thank C. Schuh (Northwestern University) for useful discussions.

## References

[1] F.H. Froes, D. Eylon, C. Suryanarayana, JOM (1990) 26–29.
[2] O.N. Senkov, J.J. Jonas, F.H. Froes, JOM (1996) 42–47.
[3] T.G. Nieh, J. Wadsworth, O.D. Sherby, Superplasticity in Metals and Ceramics, Cambridge, 1997.

[4] D.C. Dunand, in: T. Chandra, T. Sakai (Eds.), Proceedings of the International Conference on Thermomechanical Processing of Steels and Other Materials, TMS, Warrendale, 1997, pp. 1821–1830.
[5] G.W. Greenwood, R.H. Johnson, Proc. Roy. Soc. London 283 (1965) 403–422.
[6] D.C. Dunand, C.M. Bedell, Acta Mater. 44 (1996) 1063–1076.
[7] C. Schuh, D.C. Dunand, Scripta Mater. 40 (1999) 105–1312.
[8] P. Zwigl, D.C. Dunand, Metall. Mater. Trans. 29 (1998) 2571–2582.
[9] A.D. McQuillan, Proc. Roy. Soc. London 204 (1951) 309–323.
[10] H.J. Frost, M.F. Ashby, Deformation-mechanism Maps: The Plasticity and Creep of Metals and Ceramics, Pergamon Press, New York, 1982.
[11] M. Frary, C. Schuh, D.C. Dunand, Phil. Mag., in press.
[12] H.E. McCoy, Trans. ASM 57 (1964) 743–746.
[13] D.C. Dunand, S. Myojin, Mater. Sci. Eng. 230 (1997) 25–32.
[14] Y.C. Chen, G.S. Daehn, R.H. Wagoner, Scripta Metall. Mater. 24 (1990) 2157–2162.
[15] D.C. Dunand, P. Zwigl, US Patent 6 042 661 (2000).
[16] T.R.P. Gibb Jr., H.W. Kruschwitz Jr., 72 (1950) 5365–5369.
[17] H. Wipf (Ed.), Hydrogen in Metals, Vol. III, Springer, Berlin, 1997.
[18] M.Y. Wu, J. Wadsworth, O.D. Sherby, Metall. Trans. A 18 (1987) 451–462.
[19] D.C. Dunand, L. Felberbaum, Unpublished research, 2000.